IAHR AIRH

25th IAHR International Symposium on Ice
Trondheim, 23 - 25 November 2020

Physical and mechanical properties of ice from a refrozen ship channel ice in Bay of Bothnia

Vasiola Zhaka [1,*], Victoria Bonath [1], Bjørnar Sand [2], Andrzej Cwirzen [1]

[1] Luleå University of Technology, Sweden, [2] Northern Research Institute Narvik, Norway

vasiola.zhaka@ltu.se, victoria.bonath@ltu.se, bjoernar.sand@norut.no, andrzej.cwirzen@ltu.se

Winter navigation in the North Sea is expanding with respect to vessel size and traffic volume. Icebreakers create routes for ice-going vessels by breaking the level ice cover. Repeated vessel passages in the fairways and harbors initiate the formation of brash ice. The brash ice has the ability to refreeze quickly. In the current work, a field study was conducted on a refrozen brash ice ship channel located in Marjaniemi harbor in Bay of Bothnia. Aim of this study is to evaluate the structure and the strength of ice in the fully refrozen ship channel. Ship channel geometry, ice temperature and salinity were assessed in the field. The ice thickness was in average 45 cm covered by a snow layer with an average of 20 cm. The temperature profiles showed approximately -15^{O}C at the ice surface and close to 0^{O}C in the depths above 10 cm. Salinity varied from 0 to 1.5 ppt. Ice texture, density and compressive strength of refrozen brash ice were measured in the laboratory on 200 mm diameter cores. The behavior of refrozen brash ice with random ice texture was more ductile and stronger in uniaxial compression compared to the adjacent level ice.

1. Introduction

Bay of Bothnia located in the northern basin of Gulf of Bothnia is subjected to sea ice formation during winter season. The ice layer reaches its maximum thickness from February till early March (Kujala and Arughadhoss, 2012). Navigation in fairways and harbors break and erode the initial ice layer into ice pieces known as brash ice. Accumulation and growth of brash ice in frequently navigated channels occur faster than the growth of undisturbed ice layer. Heavy brash ice accumulation makes the navigation harder and unsafe (Mellor, 1980).

After each vessel passage the cold brash ice pieces submerges in the warmer water that causes heat loss and subsequently ice growth (Sandkvist, 1980). The brash ice regain strength between two vessel passages due to refreezing process. Thus, when a ship channel is subjected to very low temperatures for a long time, the full consolidation of the brash ice can occur and its breaking becomes harder (Greisman, 1981). The sailing resistance in a brash ice channel was found to be proportional with the brash ice thickness (Kitazawa and Ettema, 1985). Field measurements from a brash ice channel located in Bay of Bothnia, Luleå coast conducted by (Sandkvist, 1986) showed that the thickness of brash ice after 33 ship passages was 2.5 m.

The physical and mechanical properties of the refrozen brash ice are not well known and their study can give insight in the history of brash ice development. The detailed evaluation of properties and behavior of brash ice are necessary to develop accurate models (Riska et al., 2019). On the other hand, accurate models can assist the establishment of ice management strategies in ports and fairways (Bridges et al., 2020). The current work present results obtained from specimens sampled in a refrozen ship channel in Bay of Bothnia. The term refrozen ship channel refers to a brash ice filled channel that was consolidated prior to sampling due to navigation ban. The aim of this study was to characterize the physical and the mechanical properties of refrozen brash ice from the material perspective and compare these properties with the adjacent level ice. The investigation of refrozen brash ice properties can give a better understanding for brash ice formation and accumulation in the ship channels.

2. Measurements

2.1 Field measurements

Fully consolidated brash ice and sea level ice located at Marjaniemi Harbor in Bay of Bothnia were investigated during February 2019. Nine ice cores with 200 mm diameter were drilled along the consolidated ship track and seven cores were drilled along adjacent level ice. The distance between measuring points was 2 m. The top part of ice cores and the position in the profile were marked and the ice cores were placed in plastic bags and were transported quickly from the field to a freeze box. The samples were stored in -20^{O}C until laboratory tests were conducted in December 2019. The thickness and structure of the channel was measured by mechanical drilling with a 50 mm auger. A measuring stick with a horizontal protrusion at one end was used to measure the ice thickness in each hole and the gaps between the ice blocks. Vertical ice salinity and ice temperature profiles were measured at 2 points along the measured channel cross-section. Measurements of ice salinity and temperature profiles were done on 70 mm ice cores. For salinity measurements, the ice core was cut into 5 cm thick slices, stored in plastic bags and melted in room temperature. Mettler Toledo pH meter apparatus was used to measure the salinity of the melted sea ice based on conductive properties of the dissociated salts in water.

2.2 Laboratory tests

Ice cores were stored for 10 months in the laboratory at -20^{O}C, until the sample preparation was conducted. Unconfined compressive strength was measured for 26 samples of refrozen brash ice and for 20 sample of level ice. The ice cores were removed from the freezing box 2 hours before the sample preparation started and were stored during this time in a refrigerator room that maintained a constant temperature of -10^{O}C. Cylinders with an approximate diameter of 70 mm and height of 170 mm were drilled horizontally along the 200 mm ice cores. The depth of sampling was determined for each cylinder. Specimens were sawed to level the surface and were smoothed with fine sandpaper to reduce the radial restraint that can be caused from the steel plates applied at the top and bottom of the ice samples during compressive tests. Diameter, height and weight of samples were measured to determine the ice density. Thin slices were cut using a band saw from the cores to study the ice texture. Ice slices were stored in the refrigerator for one day in order to achieve clearer texture results. Pictures of ice texture were recorded under crossed polarized light. The test set up for the unconfined uniaxial compression and calibration of system deformation for different load levels are shown in Figure 1 and were described in details by (Bonath et al., 2019). During the compression tests, the temperature of the ice samples varied from -6^{O}C to a minimum of -13^{O}C. The ice samples where compressed at strain rates from 10^{-1} to 10^{-4} s^{-1}. After the horizontal uniaxial compression tests, specimens were stored in plastic bags and melted in the room temperature. Salinity measurement were done for each sample. The total porosity was calculated as the sum of air and brine relative volume (Cox and Weeks, 1983). The brine, pure ice and solid content were expressed as a function of temperature valid for temperatures within the range of -2^{O}C to -22.9^{O}C. The relative brine volume was computed as the ratio between the measured sea ice density and salinity with the empirical temperature function and the relative air volume were computed as the difference of the total sea ice bulk fraction with brine, ice and solid salt relative volumes.

3. Results and discussion

3.1 Properties and texture of sea ice

The sea ice salinity measured in field was relatively low, between 0 and 1.5 ppt (Figure 2). One reason is that the Bay of Bothnia generally consists of brackish water with low salinity that varies within the range of 2.5 to 4.5 ppt (Marmefelt and Omstedt, 1992). Despite that, a high amount of snow ice was observed on top of the ice cover contributing to sea ice with low salinity. Salinity measured in the laboratory after samples were stored for 10 months were even lower between 0 to 0.7 ppt. The observed difference indicated a brine loss due to brine drainage. Possibly occurred in the field due to physical transportation of the cores from the sampling area to the freezing box where samples were stored. The distance was approximately 500 m. Brine drainage does not change the total porosity of the sea ice but affects it by increasing the air volume and decreasing the brine volume. No significant correlation was observed between the salinity and the depth. The ice temperature was generally close to zero, due to a warm period with air temperatures constantly above zero during the week before the measurements. The air temperature during sampling was approximately -15°C, thus the uppermost ice layer had the ice temperatures colder than 0°C, Figure 2.

Refrozen brash ice (RBI) and level ice (LI) texture was investigated by recording images of thin ice sections under cross-polarized light. In both studied sea ice types RBI and LI, it was observed a mixed ice structure of granular and columnar ice. Figure 3 shows representative

images of horizontal and vertical profiles for both refrozen brash ice and level ice. The microstructure of 8 RBI cores were investigated from the 9 cores sampled in total. Two different types of mixed ice were noticed in the RBI samples. The first type contained mainly randomly orientated fragments of columnar ice crystals with sizes varying from 1 up to 10 cm, mixed with granular crystals of sizes smaller than 1 cm. The second type of the observed ice mainly contained granular ice crystals of sizes smaller than 1 cm mixed with some crystals bigger than 1 cm. The second type containing mainly granular crystals was recorded in five from the 8 cores investigated while in the three other cores both microstructure types were observed. The high amount of granular ice maybe subjected to snow ice imply the possibility of the RBI thicknesses increase due to snowfall. The hypothesis that a significant increase in RBI thickness occurs due to snowfall agitation with brash ice during vessel passages should be further investigated. In addition, the snow-ice effect in the brine change due to agitation and refreezing process in channels should be further studied. Six cores of LI were observed under cross-polarized light. Level ice contained vertically orientated crystals of columnar ice that were interrupted from possible frazil ice entrapped beneath the ice cover. In all six cores investigated, the frazil ice layers were present. Columnar ice regrowth occurred after these interruptions. Based on the level ice and ridges texture classification presented elsewhere (Bonath et al., 2019) the refrozen brash ice can be classified as $IIIB_1$ and $IIIB_2$ ice types that are described respectively as refrozen ice fragments containing small and big random crystals. Grain size of ice crystal for refrozen brash ice and level ice in the horizontal direction of viewing varied from few mm up to 10 cm. (Bridges et al., 2019) recently recorded the microstructure of the laboratory produced refrozen brash ice. The crystals had random orientation and size variation.

3.2 Uniaxial compression and stress strain curves

Deformation history of compression test and crack propagation within ice samples were observed to have a high impact on the maximum strength (Sinha, 1982). The loading history during uniaxial compression test was studied and representative stress-strain curves are presented in Figure 4. Refrozen brash ice and level ice showed a brittle behavior at high strain rates equal to $10^{-2}s^{-1}$. Brittle behavior could be related to the immediate loss of the loading capacity after reaching the maximum compressive strength (Moslet, 2007). The level ice showed both brittle and ductile behaviors for strain rates equal to 10^{-3} and 10^{-4} s^{-1}. Ductile behavior can be described as the ability of ice to bear the load after the maximum strength is achieved and was observed in the stress-strain curves as the softening branch occurring after the maximum compressive strength. The refrozen brash ice showed a ductile behavior for strain rates of 10^{-4} s^{-1} and $10^{-3}s^{-1}$. In addition, a clear transition zone between brittle and ductile behavior was present. The studied RBI samples showed a ductile behavior in a bigger number of samples compare to level ice. The intrinsic properties of ice like the grain size, temperature and porosity could affect the behavior variation of LI and RBI samples. Earlier study indicated that the ice fracture under the uniaxial compression was affected by the stress state at the ice-platen interface (Schulson et al., 1989). In the current work to reduce this effect, the ice surface was smoothened. The splitting failure was common for all the samples with brittle behavior leading to a uniform internal damage. In the case of the ductile failure, the cracking nucleated and scattered to random sites in the sample leading to a failure without splitting. The uniaxial compression strength results for different loading rates and the standard deviation are presented in Table 1. The average compressive strength for 16 LI samples was 4.05 MPa. The refrozen brash ice had an average compressive strength of 5.04 MPa for 23 samples. Three samples of refrozen brash ice and for samples of level ice were not evaluated due to possible measurement errors. The uniaxial compression in the horizontal

loading direction showed higher average strength values for the refrozen brash ice with granular and randomly oriented columnar grains compare to the level ice. Earlier studies by (Schulson, 1990) showed that decreasing the strain rate up to $10^{-3}s^{-1}$, the grain size and the temperature tended to increase the maximum compressive strength for fresh water granular ice with a brittle behavior. The compressive strength of the sea ice decreased with decreasing the strain rate below $10^{-3}s^{-1}$ (Timco and Frederking, 1990). In the present work, the same trend was observed for RBI samples that had higher ultimate compressive strength for strain rate equal to $10^{-3}s^{-1}$ and a lower ultimate compressive strength for higher and lower strain rates, Table 1 and Figure 4. On the other hand, the LI samples had a higher compressive strength for strain rates equal to $10^{-4}s^{-1}$. A possible explanation could be that the number of samples tested is small for a representative stress-stain rate trend.

Another engineering property of ice that is very commonly determined from the stress-strain curves is the elastic modulus that was determined by dividing the maximum compressive strength by the corresponding measured strain. Both level ice and refrozen brash ice showed an increase in modulus of elasticity at higher strain rate, $10^{-2}s^{-1}$. Others observed similar trends (Sinha, 1982).

3.3 Compressive strength vs physical properties

Ice physical properties have a major influence on the compressive strength. (Shafrova and Høyland, 2008) studied the compressive strength of ridges and level ice and their results for the level ice showed that the compressive strength increase with depth. The strongest ice layer was in the bottom of the ice cover. Independently of the applied strain rate the compressive strength of level ice sheet tended to increase with depth due to lower salinity in the bottom part (Timco and Frederking, 1990). Recently the compressive strength for laboratory grown refrozen brash ice was reported to be higher in the top layer compare to the bottom layer (Bridges et al., 2019). The variation of uniaxial compressive strength of refrozen brash ice and level ice with depth and different strain rates is shown in Figure 5. The compressive strength appeared to be higher for samples taken from depths between 15 and 40 cm. In the present case, the compressive strength was probably lower in the top due to snow ice presence.

No clear dependency between the ice porosity and the depth was observed in any of the ice types in this study, Figure 5. All the samples of the refrozen brash ice taken from the depth between 15 and 40 cm had very low porosity. Similar trends were observed in the case of the level ice. The calculated average density of the studied level ice samples was 0.893 g/cm^3 and for the refrozen brash ice was 0.897 g/cm^3. The refrozen brash ice samples had a higher slightly calculated average density. Average porosity, average density and density standard deviations for a certain number of samples are shown in Table 1. The relation of maximum compressive strength with total porosity, air and brine relative volume is shown in Figure 6. The total porosity was computed as the sum of brine and air relative volume (Cox and Weeks, 1983). The results showed that the effect of those parameters on the measured compressive strength were in the same trend as the results presented by others (eg, Moslet, 2007; Shafrova and Høyland, 2008; Timco and Frederking, 1990), where the sea ice compressive strength increased with decreasing porosity. In the current work, the brine volume did not had the main influence in the total porosity. The air volume was the main contributor to the total porosity of refrozen brash and level ice, Table 1. The correlation between the maximum strength and the total porosity was evaluated by using the equation 1 for the horizontal loading direction (Moslet, 2007). Equation 2 was used previously to

evaluate the compression strength of granular ice for strain rate equal to$10^{-3}s^{-1}$ (Timco and Frederking, 1990):

$$\sigma = A \cdot \left(1 - \sqrt{\frac{\nu_T}{B}}\right)^2 \quad \textbf{[1]}$$

$$\sigma = 49(\dot{\varepsilon})^{0.22}\left[1 - \sqrt{\frac{\nu_T}{0.28}}\right] \quad \textbf{[2]}$$

A and B are empirical coefficients. (Timco and Frederking, 1990) described B as the total ice porosity that causes the ice maximum strength to approach zero. For the granular ice, B was 0.28 and for columnar ice, B was held constant at 0.7 (Moslet, 2007). Coefficient A was introduced as a constant that depends on loading direction and ice temperature (Bonath et al., 2019). Fitting curves for the maximum compressive strength for the refrozen brash ice and level ice are shown in Figure 7. The maximum compressive strength of ice samples decreased with increasing the total porosity. On the present fitting curves for level ice the best fit had an A equal to 8 and for the refrozen brash ice the best fit had an A equal to 12.5.

4. Conclusions

Refrozen brash ice and level ice properties were studied for cores sampled during winter 2019 in Marjaniemi harbor in Bay of Bothnia. Horizontal uniaxial compression were evaluated for 23 samples of RBI and 16 samples of LI. Sea ice density was computed from the mass - volume method. Total porosity was computed as the sum of brine and air relative e volume. Sea ice texture was assessed from pictures of ice yielded under cross-polarized light.

1. Two types of microstructure were recorded in refrozen brash ice samples. The first type with higher amount of big randomly orientated crystals was in a smaller proportion compare to the second type with a higher amount of small random crystals. Level ice microstructure contained mainly elongated ice crystals with a vertical crystal growth. RBI structures were similar to the IIIB1 and $IIIB_2$ ice structures observed by (Bonath et al., 2019).

2. Refrozen brash ice samples were stronger in horizontal direction compare to the adjacent level ice and showed a higher ductility than level ice. LI maximum compressive strength increased with decreasing strain rate. RBI maximum compressive strength was higher for strain rates of $10^{-3}s^{-1}$, where the transition from brittle to ductile occurred. Both ice types exhibit a brittle behavior in strain rates equal to $10^{-2}s^{-1}$. Refrozen brash ice samples showed only ductile behavior for strain rates equal to $10^{-3}s^{-1}$. Level ice for strain rates from 10^{-3} to $10^{-4}s^{-1}$ showed both brittle and ductile behavior.

3. For both level ice and refrozen brash ice sampled in Bay of Bothnia the maximum compression strength decreased with increasing porosity. Brine volume was very low and its influence in total porosity and maximum strength was probably lower than air volume.

Acknowledgment

This work was supported by the Kolartic Project ICEOP in collaboration with the 5th Snow science winter school 2019, Hailouto, Finland.

References

Bonath, V., Edeskär, T., Lintzén, N., Fransson, L., and Cwirzen, A., 2019. Properties of Ice from First-Year Ridges in the Barents Sea and Fram Strait. Cold Regions Science and Technology 168, 102890.

Bridges, R., Riska K., and Haase A., 2019. Experimental Tests on the Consolidation of Broken and Brash Ice. Proceedings of the 25th International Conference on Port and Ocean Engineering under Arctic Conditions.

Bridges, R., Riska, K., Suominen, M., and Haase, A., 2020. Experimental Tests on Brash Ice Channel Development. International Society of Offshore and Polar Engineers.

Cox, G.F.N., and Weeks W.F., 1983. Equations for Determining the Gas and Brine Volumes in Sea Ice Samples. CRREL Report: US Army Cold Regions Research and Engineering Laboratory. 29(102),306–16.

Greisman, P., 1981. Brash Ice Behavior. U.S. Coast Guard Research and Development Center: Report No. USCG-D-30-81.

Kitazawa, T., and Ettema R., 1985. Resistance to Ship-Hull Motion through Brash Ice. Cold Regions Science and Technology 10(3), 219–34.

Kujala, P., and Sankar A., 2012. Statistical Analysis of Ice Crushing Pressures on a Ship's Hull during Hull-Ice Interaction. Cold Regions Science and Technology 70, 1–11.

Marmefelt, E., and Omstedt, A., 1992. Deep water properties in the Gulf of Bothnia. Continental Shelf Research 13(2-3), 169-187.

Mellor, M., 1980. Ship Resistance in Thick Brash Ice. Topics in Catalysis 3(4), 305–21.

Moslet, P. O. 2007. Field Testing of Uniaxial Compression Strength of Columnar Sea Ice. Cold Regions Science and Technology 48(1), 1–14.

Riska, K., Bridges, R., Shumovskiy, S., Thomas, C., Coche, E., Bonath, V., Tobie, A., Chomatas, K., and Oliveira, R.C.D., 2019. Brash Ice Growth Model – Development and Validation. Cold Regions Science and Technology 157, 30–41.

Sandkvist, J., 1980. Observed growth of brash Ice in ship's tracks. Research Report Series. Water Resources Engineering University of Lulea, Lulea, Sweden.

Sandkvist, J., 1986. Brash ice behaviour in frequented ship channels. Water Resources Engineering. Research Report Series A, No.139 Luleå University of Technology, Luleå, Sweden.

Schulson, E. M. 1990. The Brittle Compressive Fracture of Ice. Acta Metallurgica Et Materialia 38(10), 1963–76.

Schulson, E. M., M. C. Gies, G. J. Lasonde, and W. A. Nixon. 1989. The Effect of the Specimen-Platen Interface on Internal Cracking and Brittle Fracture of Ice under Compression: High-Speed Photography. Journal of Glaciology 35(121), 378–82.

Shafrova, S., and Høyland K.V., 2008. Morphology and 2D Spatial Strength Distribution in Two Arctic First-Year Sea Ice Ridges. Cold Regions Science and Technology 51(1),38–55.

Sinha, N. K. 1982. Constant Strain- and Stress-Rate Compressive Strength of Columnar-Grained Ice. Journal of Materials Science 17(3),785–802.

Timco, G.W, and Frederking R.M.W., 1990. Compressive Strength Of Sea Ice Sheets. Cold Regions Science and Technology 17(3), 227–240.

Table 1. Summary of test results for refrozen brash ice and level ice under different strain rates, number of samples tested, avarage maximum compressive strength, standard deviation for the maximum compressive strength, avarage measured salinity, avarage relative air and brine volume, total porosity, avarage ice density and the standard deviation for the ice density.

Nr.Samples		Strain Rate (s^{-1})	σ_{max} (Mpa)	σ_{std} (Mpa)	S (ppt)	ν_a (-)	ν_b (-)	ν_t (-)	ρ_{avg} (g/cm^3)	ρ_{std} (g/cm^3)
RBI	4	$1.1 \cdot 10^{-2}$	4.89	1.26	0.35	0.008	0.002	0.010	0.912	0.004
	4	$1.1 \cdot 10^{-3}$	6.29	0.67	0.37	0.037	0.002	0.039	0.884	0.019
	5	$1.1 \cdot 10^{-4}$	4.16	1.61	0.36	0.010	0.019	0.012	0.910	0.006
LI	3	$5.3 \cdot 10^{-2}$	2.90	0.71	0.39	0.048	0.002	0.050	0.874	0.084
	3	$1.1 \cdot 10^{-3}$	4.47	1.19	0.26	0.034	0.001	0.035	0.888	0.020
	3	$5.3 \cdot 10^{-4}$	5.09	0.74	0.32	0.023	0.002	0.025	0.897	0.013

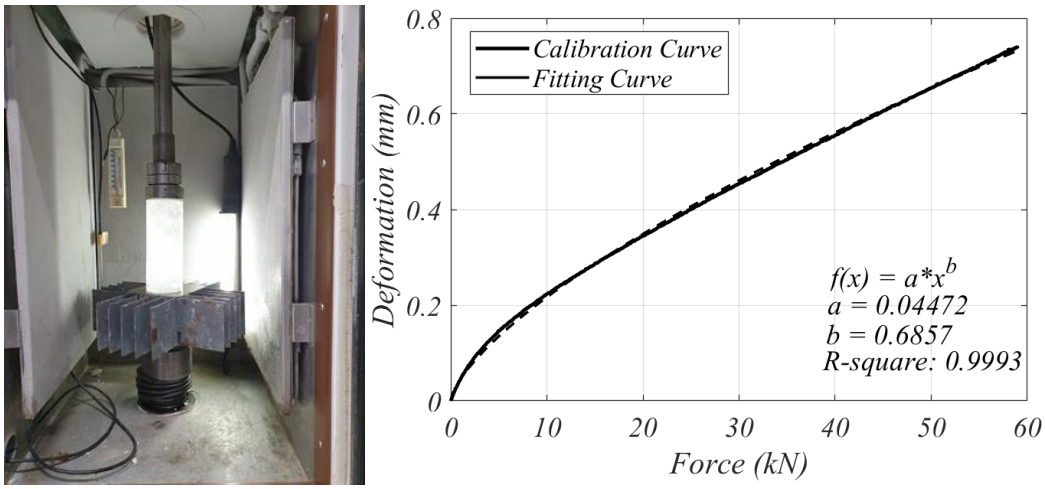

Figure 1. Unconfined uniaxial test set up and deformation calibration curve.

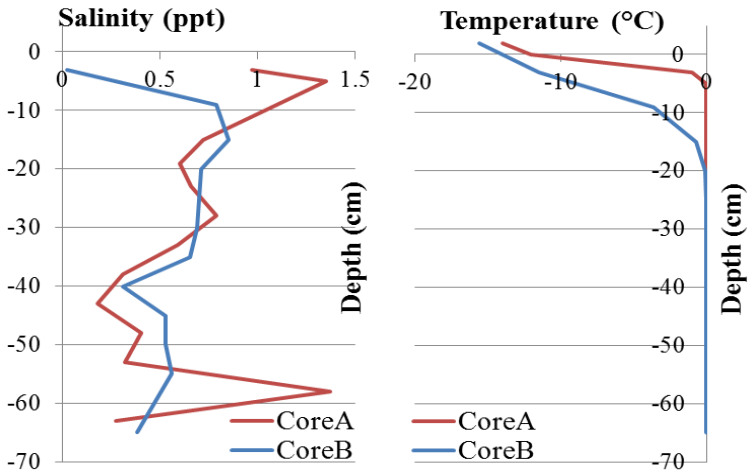

Figure 2. Salinity and temperature profile for refrozen brash ice sampled at two different positions.

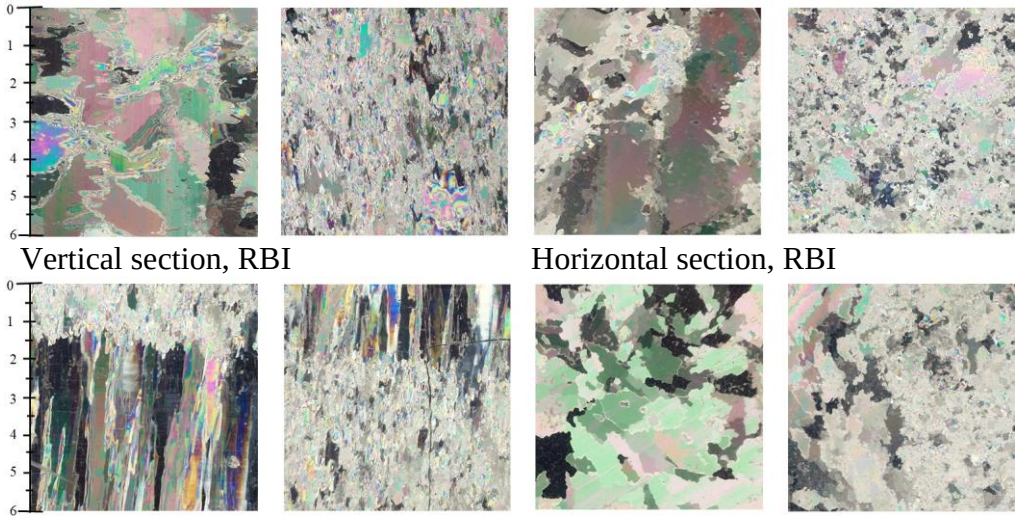

Figure 3. Texture of refrozen brash ice (RBI) and level ice (LI) observed under cross-polarized light in vertical and horizontal direction. Appeared scale represents a microstructure equal to 6x6 cm.

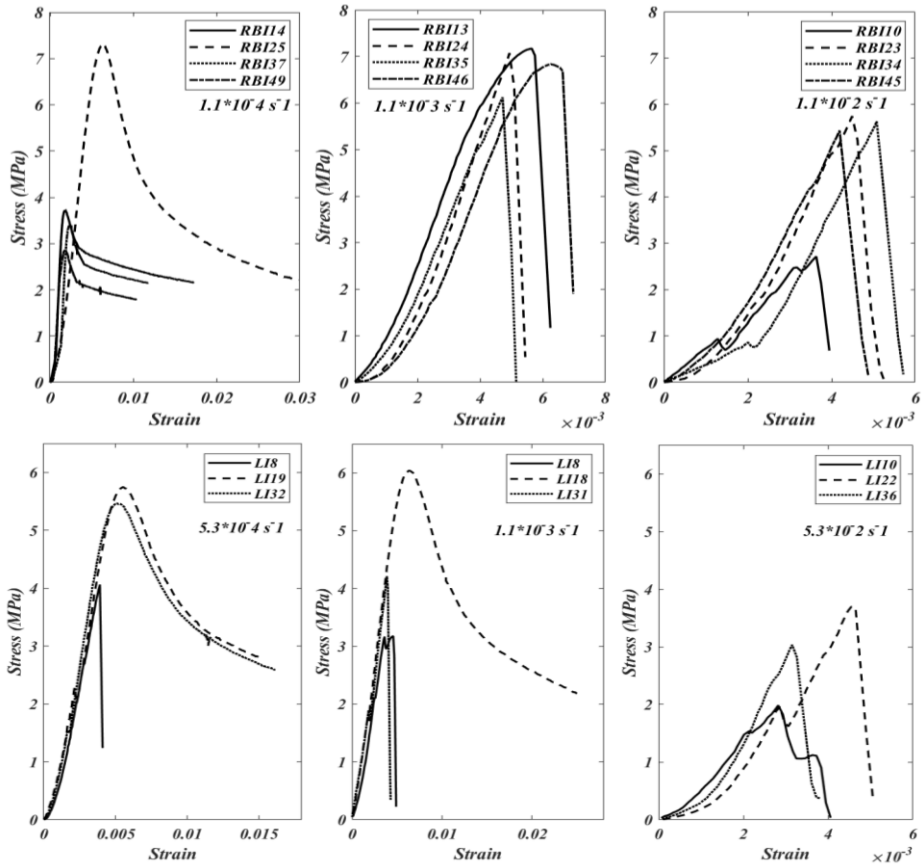

Figure 4. Stress-strain curves for the refrozen brash ice (RBI) and level ice (LI) in different strain rates and sampled in different depths in cm, indicated from numbers in the legends, i.e RBI10 was refrozen brash ice specimen sampled in the depth of 10 cm.

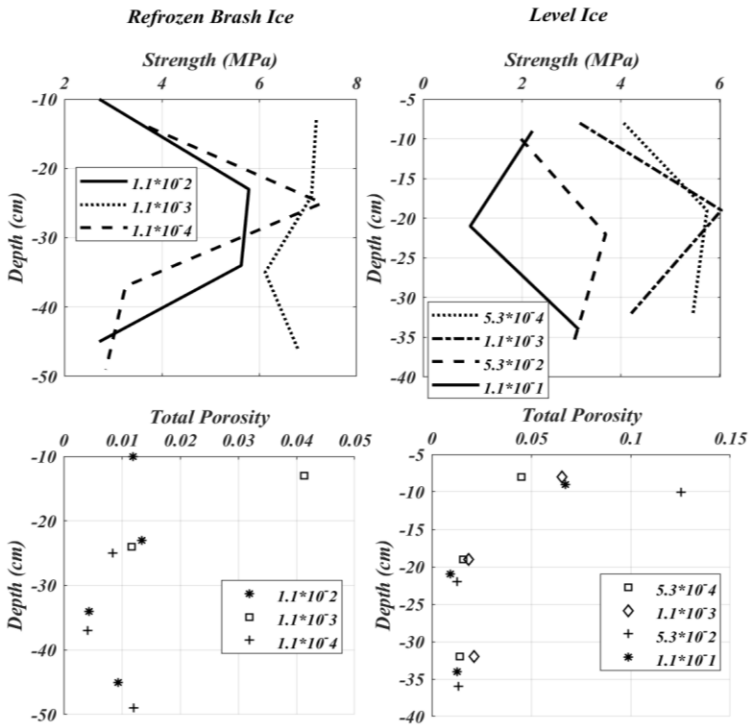

Figure 5. Maximum compressive strength and total porosity variation of refrozen brash ice and level ice with the depth**.**

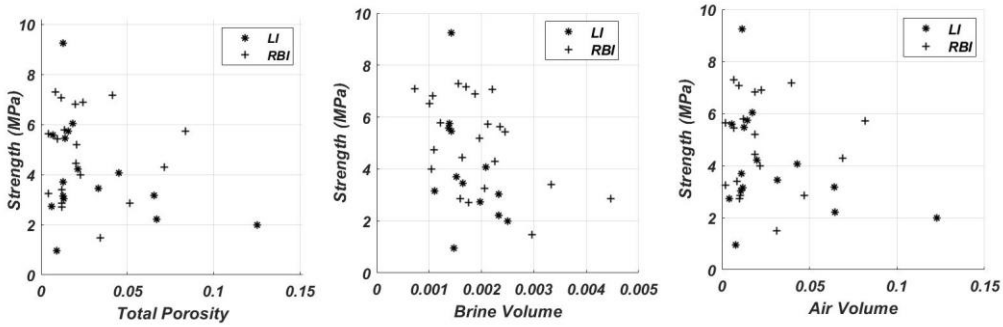

Figure 6. Compressive strength vs total porosity, relative brine volume and relative air volume for refrozen brash ice and level ice.

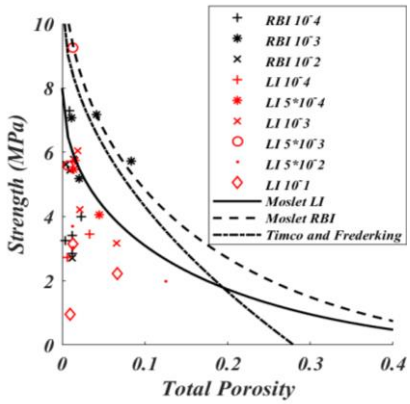

Figure 7. Maximum compressive strength presented as function of total porosity.